REE/trace element characteristics of sandstone-type uranium deposits in the Ordos Basin*

LING Mingxing (凌明星)[1,2], YANG Xiaoyong (杨晓勇)[1,2**], SUN Wei (孙卫)[3], MIAO Jianyu (苗建宇)[3], and LIU Chiyang (刘池阳)[3]

[1] *CAS Key Laboratory of Crust-Mantle Materials and Environments, School of Earth and Space Sciences, University of Science and Technology of China, Hefei 230026, China*

[2] *Research Center of Oil and Natural Gases, University of Science and Technology of China, Hefei 230026, China*

[3] *Department of Geology, Northwest University, Xi'an 710069, China*

Abstract The major elements, trace elements and REEs were analyzed on the samples collected from the sandstone-type uranium deposits in the Ordos Basin to constrain the mechanism of uranium enrichment. The total REE amount ranges from 36.7 to 701.8 μg/g and the REE distribution patterns of the sandstone-type uranium samples are characterized by LREE enrichment and high REE depletion. The results also indicated a high Y abundance and Eu anomalies between 0.77−1.81. High-precision ICP-MS results showed that U abundances are within the range of 0.73−150 μg/g, showing some strong correlation between U enrichment and related elements such as Ti, V, Zr, Mo, and Au. In addition, Th abundance is correlated with ΣREE.

Key words sandstone-type uranium deposit; REE; trace element; Ordos Basin

1 Introduction

The Ordos Basin is the second largest sedimentary basin in China. During the last 10 years, a great progress has been achieved in the aspects of tectonic evolution, dynamics process, inner and outer geological processes during Mesozoic-Cenozoic times, and effects on multi-energy mineral resources, environmental protection and earthquake in this basin (Ye and Lu, 1997; Zhang Lifei et al., 1998; Liu Shaofeng, 1998; Zhang Jin et al., 2004; Darby and Ritts, 2002; Li Xianqing et al., 2003a, b; Ritts et al., 2004; Liu Chiyang et al., 2005; Dai Jinxing et al., 2005; Yang Xiaoyong et al., 2006).

The extensional exploration in combination with studies both at home and abroad indicates that the 4 extraordinary significant energy resources: oil, gas, coal and uranium, which have an affinity with the national economy and people's livelihood, coexist mainly in sedimentary basins. The sandstone-type uranium deposits are one of the first discovered uranium deposit types in the world (Granger et al., 1961), and then discovered and reported in all continents throughout the world. In fact, the sandstone-type uranium deposits in basins are distributed all over the world. However, according to the number of uranium deposits or the total reserves, they are distributed predominantly in the Northern Hemisphere between latitudes 25 to 50 degrees, especially in the Mid-East Asian huge metallogenic belt. The belt covers an area extending from the Songliao Basin in China in the east to the Caspian Sea in the west with an extension of 6000 km (Peng Xinjian et al., 2003; Li Shengfu and Zhang Yun, 2004; Chen Daisheng et al., 2003; Yang Dianzhong et al., 2004; Liu Chiyang, 2005; Min Maozhong et al., 2005). The Ordos Basin is abundant in diverse energy resources and useful mineral resources. Therefore, it is of profound scientific significance and industrial value to study the basin.

Along with deep-going ore exploration and theoretical research, *in-situ* leachable sandstone-type uranium deposits and mineralization abnormities have

ISSN 1000-9426

* This study is supported by the Chinese 973 National Key Research and Development Program (2003CB214606) on Accumulation and Formation of Multi-Energy Mineral Deposits Coexisting in the same Basin and Open Foundation of the State Laboratory of Geological Processes and Mineral Resources.

** Corresponding author, E-mail: xyyang@ustc.edu.cn

been discovered in many locations in the Ordos Basin. For example, discovery of the Dongsheng large-scale uranium deposit, characterized by great reserves and perspective for a super-large deposit, marks an important breakthrough in the exploration of the *in-situ* leachable sandstone-type uranium deposits (Di Yongqiang, 2002; Cheng Fazheng, 2002; Zhu Xiyang et al., 2003; Xiao Xinjian et al., 2004a, b).

In this study, we made a systematical analysis on samples from the sandstone-type uranium deposits in the Ordos Basin, including the abundances of REE, trace elements and several major elements, in an attempt to discuss the mechanism of uranium enrichment in this basin and the substantial relations among and furthermore the rules of coexistence of multi-energy mineral deposits in the same basin.

2 Geological background and characteristics of the uranium deposits

The Ordos Basin is also called the Shaan (Shaanxi)-Gan (Gansu)-Ning (Ningxia) Basin, and its main portion covers an area of 2.5×10^5 square kilometers. The Yimeng Uplift in the north, the Weibei Uplift in the south, the West Fold and Fault Belt in the west, and the Western Shaanxi Flexure Belt in the east constitute a unique structure pattern (Fig. 1). Oil and gas reservoirs are estimated at 86×10^8 tons and 11×10^{12} cubic centimeters, respectively (Hu Wenrui, 2000), in which the reserves of oil rank the third of the basins abundant in oil and gas resources, only next to the Bohai Bay Basin and Songliao Basin (Liu Chiyang, 2005). The present Ordos Basin is attributed to be a remnant craton basin in the Mesozoic (Zhao Chongyuan and Liu Chiyang, 1990).

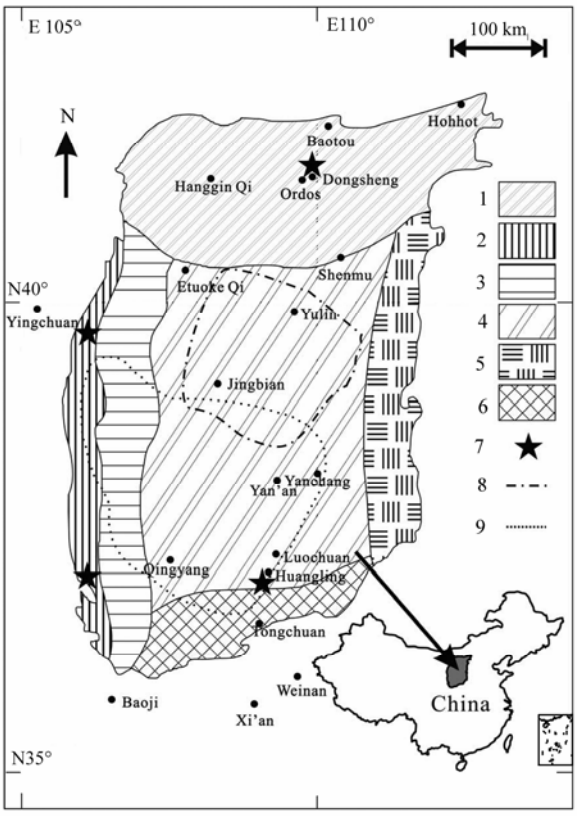

Fig. 1. Geological sketch map of the Ordos Basin and its relative geographical position in China (After Wu Rengui et al., 2003; Wei Yongpei and Wang Yi, 2004; Xie Chenxia, 2004). 1. Yimeng Uplift; 2. Western Fold and Fault Belt; 3. Tianhuan Syncline; 4. Yishan Slope; 5. Western Shaanxi Flexure Belt; 6. Weibei Uplift; 7. uranium deposit and sample locality; 8. middle gas field zone; 9. Yanchang Formation oil-bearing zone.

The early evolution of the Ordos Basin is marked by a particular process in which uplifting proceeded gradually at the eastern edge of a paleo-basin with the eastern boundary of sedimentation moving westwards. As a result, the former sediments were eroded (Zhao Chongyuan and Liu Chiyang, 1990). Till Late Jurassic, the residual basin showed such a pattern as to be lower in the west and higher in the east. In the late Early Cretaceous, the Ordos Basin died out as a result of unitary rise. During the long-term evolution and deformation, the Ordos Basin had experienced overall ascending and descending, while internal vertical movements were comparatively weak. Furthermore, intense tectonic activities, as well as basin deformation, occurred at the edge of the Ordos Basin (Liu Shaofeng, 1998; Zhang Jin et al., 2004; Darby and Ritts, 2002; Ritts et al., 2004; Liu Chiyang et al., 2005). Deformation during the evolution of the Ordos Basin made multi-energy mineral deposits coexisting and emplacement in the same basin (Liu Chiyang, 2005).

Recently, many uranium deposits have been discovered in the Ordos Basin, of which the Dongsheng uranium deposit in the northeast is largest in scale, highly expected to be a super-large deposit. U-Pb isochron age of sandstone samples from the Dongsheng uranium deposit is 107±16 Ma, which may represent the paleo-oxidation time when uranium was enriched and precipitated (Xia Yuliang et al., 2003).

The ore-bearing strata in the Dongsheng sandstone-type uranium deposit are represented by the Zhiluo Formation which can be classified as the upper and lower segments. The lower segment was further divided into two sub-segments. The lower sub-segment is composed of ore-bearing gray sandstone and the upper sub-segment is composed mainly of green sandstone and mudstone. The upper segment consists of variegated medium to fine -grained sandstones and mudstones. The rocks are loose, with the sand body measuring 20–40 meters in thickness. Developed in the ore-bearing sand body is an oxidation zone-oxidation reduction zone-reduction

zone layered petrochemical zone from north to south. The oxidation zone is yellowish in color on the Earth's surface, though it is celandine green or powder blue in drills. The oxidation- reduction frontier plane extends east-westwards in the mass, exhibiting a complex S-pattern. The oxidation-reduction transition zone is

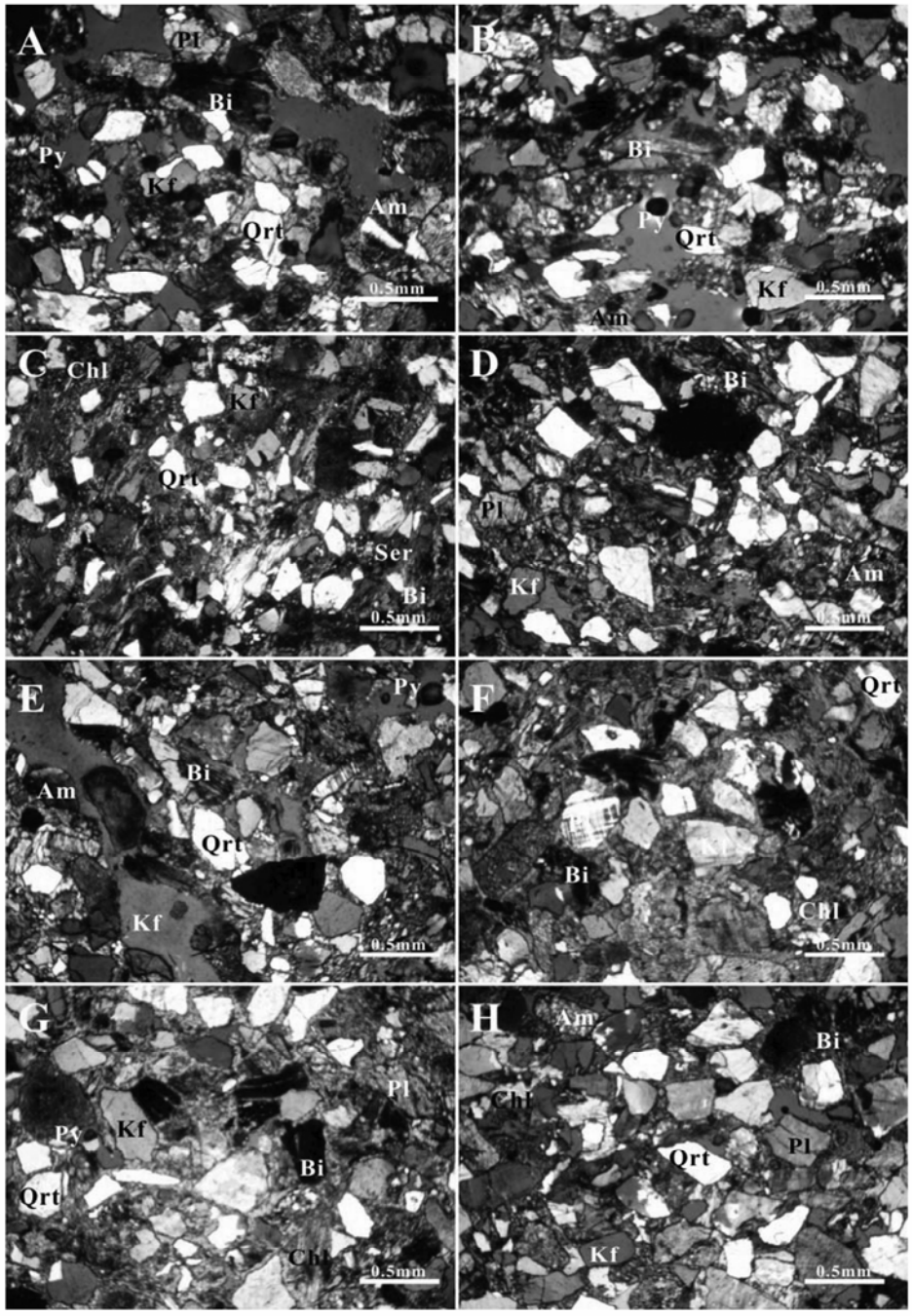

Fig. 2. Partial results of slice observation of the sandstone-type uranium deposits in the Ordos Basin. Qrt. quartz; Pl. plagioclase; Kf. potassic feldspar; Bi. biotite; Am. amphibole; Ser. sericite; Chl. chlorite; Py. pyrite. Scale bar: 0.5 mm. A. ZK341-60-03, medium-grained feldspar sandstone, strong paulopost alteration of feldspar and chloritization observed; B. another microscopic image of ZK341-60-03; C. ZKA183-87-11, muddy fine sandstone with grain diameter between 0.1−0.3 mm, there exist a few fibrous products of paulopost alteration like sericite and chlorite; D. ZKA183-87-08, medium-coarse-grained quartz sandstone composed of approximately 50% quartz and 35% feldspar; chloritization and sericitization are also in existence. Some microlites of carbonate minerals appear in the form of cements; E. another microscopic image of ZKA183-87-08; F. ZKA95-11-09, coarse-grained feldspar sandstone, there are tenuous feldspar grid twins and plagioclase multiple twins, a proportion of which was altered into chlorite, muscovite and biotite coexist, and the latter resulted from paulopost alteration; G. A39-14-03, medium-grained feldspathic quartz sandstone with 60% quartz; most of the quartz and feldspar grains themselves have sharp edge angles, and chloritization was observed, too; H. A39-14-04, medium-coarse-grained feldspar sandstone; biotite shows signs of having experienced deformation and feldspar grains, chloritization and sericitization; calcite grains are interstitial to the crystals.

gray or French grey, and it is rich in organic matter and nodular pyrite. The reduction zone is grey and abundant in organic matter. In addition, crystalline pyrite is visible. Uranium mineralization occurred nearby the frontier of the interlayered oxidation-reduction zone, and curved, plate-like or lentoid uranium ore bodies were recognized (Zhu Xiyang et al., 2003). Shown in Fig. 2 are the characteristics of some rock samples.

Xiao Xinjian et al. (2004a) described the features of post-alternation vertical zoning on the basis of the petrography data from the Zhiluo Formation sandstones: the lower sub-segment of the lower segment of the Zhiluo Formation, which consists of grey and hoar sandstones and is also a ore-bearing segment, possesses mainly a green color due to feldspar epidotization (I). Furthermore, carbonation was recognized. In the upper sub-segment, grey sandstone turns green mainly due to biotite chloritization (II). All the processes including feldspar chloritization, epidotization, argillation and carbonation led to the formation of the zone; the sandstone is celadon in the segment mostly because of its containing plenty of green biotite but no chlorite, and relatively high abundance of Fe^{2+} in the minerals appears to be the essential reason (Fig. 2).

3 Samples and experiments

In this study, 21 representative samples (Table 1) were collected from 8 drill holes in the Ordos Basin for study. Either extension or depth of the samples represents the universality and particularity of the sandstone-type uranium deposits in the Ordos Basin.

Of the 21 samples in this study there are 6 fine-grained quartz sandstone samples, 13 quartz sandstone samples, and 2 mudstone samples. As is known, quartz sandstone and mudstone generally and extensively exist in the sandstone-type uranium deposits. The mudstone samples were abundant in organic matter, therefore it is of great significance to determine REE and trace elements and their correlations with reference to previous studies on the relationship between organic matter and uranium enrichment (Min Maozhong et al., 2005; Milodowski et al., 1990). In addition, we can probe into the effects on uranium enrichment of granularity difference between fine-grained sandstone and normal sandstone.

REE and trace elements were determined by high precision ICP-MS Plasma Quad 3, made by the Thermo VG Elemental Company (UK), at the Physical-Chemical Lab. Center of the Univ. Sci. & Tech. The errors involved in the measurement were

Table 1. Samples and their lithologic features of the sandstone-type uranium deposit samples from the Ordos Basin

Sample type	Sample No.	Lithology
U-bearing sedimentary rock	ZK183-79-02	Celadon medium-grained sandstone
	ZK183-79-06	Celadon medium-grained sandstone
	ZK183-79-09	Celadon medium-fine-grained sandstone
	ZK183-79-12	Hoar medium-coarse-grained feldspar sandstone
	ZK341-60-04	Celadon medium-fine-grained sandstone
	ZK341-60-05	Grey muddy siltstone, containing carbonic detrital matter
	ZK64-127-S-07	Celadon medium-fine-grained feldspar sandstone
	ZKA139-35-03	Hoar medium-coarse-grained feldspar sandstone
	ZKA139-35-05	Hoar medium-coarse-grained feldspar sandstone
	ZKA139-35-13	Hoar medium-coarse-grained feldspar sandstone
	ZKA183-87-02	Celadon siltstone
	ZKA183-87-08	Grey medium-coarse-grained quartz sandstone
	ZKA183-87-09	Hoar medium-grained feldspar sandstone
	ZKA183-87-10	Hoar medium-grained feldspar sandstone
	ZKA39-14-02	Celadon mudstone
	ZKA39-14-04	Hoar medium-coarse-grained feldspar sandstone
	ZKA39-14-06	Hoar medium-coarse-grained feldspar sandstone
	ZKA79-11-05	Hoar silt-mudstone
	ZKA79-11-09	Grey medium-coarse-grained feldspar sandstone
	ZKA79-11-11	Grey medium-coarse-grained feldspar sandstone
	ZKA79-11-12	Grey medium-coarse-grained feldspar sandstone
Standard	GSR-4	Standard quartz sandstone
	GSR-5	Standard shale

maintained at 2%−5%.

Samples were ground in a carnelian mortar, as fine as 200 mesh, or so by hand to avoid contamination while a special caution was taken in grinding. First and for most, the indoor atmosphere must be kept clear and clean in order to reduce air dust contamination. Secondly, the carnelian mortar should be cleaned with analytically pure alcohol for several times and then dried before use, to avoid cross contamination among different samples. Finally, the sample powder was put into sample bags and the bags were then tightly sealed. Samples GSR-4 and GSR-5, used as the standard samples in the test, are quartz sandstone and shale, respectively.

Five mL of mixed acid of HNO_3 and HF in the proportion of 1∶5 was used in the course of dissolution. With reference to the method of Liu Ying et al. (1996), the mixed acid was favorable to thorough-going dissolution of the samples. In the late stage of dissolution, 0.5 mL of HCl_4 was added. The temperature varied from sample to sample to confirm whether all the samples were completely dissolved. During ICP-MS determination, it was necessary to add 2% HNO_3.

4 Results and discussion

4.1 REE characteristics and chondrite normalization

Because the REEs are insoluble and very low in concentration in water, the REEs present in sediments reflect the chemistry of the source. They are transported chiefly in the form of particulate matter. The most important factor affecting the REE contents of clastic sediments is the provenance (Fleet, 1984; McLennan, 1989). Thus it makes good sense to discuss REE characteristics and their distribution patterns in the samples.

The REEs consist of 14 lanthanides (except Pm) and Y. Furthermore, we made a series of numerical statistics on REE characteristic parameters, i.e., ΣREE, ΣLa-Nd, ΣSm-Ho, ΣEr-Y, LREE/HREE, ΣCe/ΣY and δEu after Wang Zhonggang et al. (1989). All these results are listed in Table 2.

Based on the data listed in Table 2, it can be seen that the REEs in the sandstone-type uranium deposits in the Ordos Basin have the following characteristic features:

As a whole, the light REEs are enriched and the heavy REEs are depleted; ΣREE fluctuates awfully between 36.7 μg/g and 701.8 μg/g; the values of ΣLa-Nd, ΣSm-Ho and ΣEr-Y are 25.3–567.3, 4.46–48.68 and 6.91–85.83 μg/g, respectively, showing an obvious trend of light REE enrichment, middle REE slight depletion and heavy REE depletion; the ratio of LREE/HREE varies greatly between 6.91−25.79; while the value of ΣCe/ΣY is relatively small, varying from 1.86 to 9.90. Since the Y abundance of the samples ranging between 5.31−69.3 is comparatively high, we can see the disparity between the two REE parameters; absolutely all the samples show remarkable positive Eu anomalies, except for two or three samples showing negative anomalies, fluctuating greatly from 0.77 to 1.81.

The general characteristics of the chondrite-normalized REE distribution patterns (Fig. 3) are light REE enrichment and heavy REE depletion. It is clear that the chondrite-normalized REE distribution patterns of all the samples are basically coincident

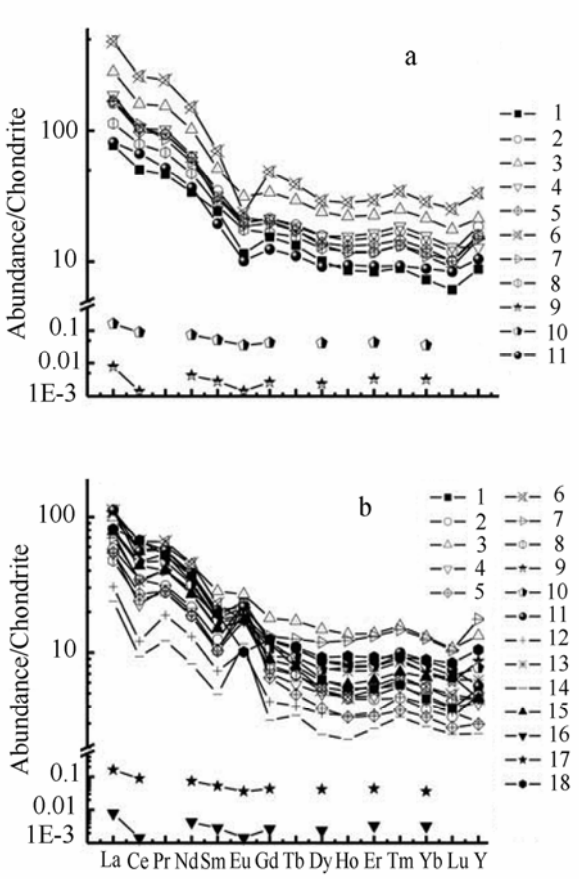

Fig. 3. Chondrite-normalized REE distribution patterns. a. Samples showing negative Eu anomalies: 1. GSR-4; 2. GSR-5; 3. ZK341-60-05; 4. ZKA139-35-05; 5. ZKA183-87-02; 6. ZKA183-87-10; 7. ZKA39-14-02; 8. ZKA79-11-05; 9. typical seawater; 10. river water; 11. upper crust. b. Samples with positive Eu anomalies: 1. ZK183-79-02; 2. ZK183-79-06; 3. ZK183-79-9; 4. ZK183-79-12; 5. ZK341-60-04; 6. ZK64-127-S-07; 7. ZKA139-35-03; 8. ZKA139-35-13; 9. ZKA183-87-08; 10. ZKA183-87-09; 11. ZKA39-14-04; 12. ZKA39-14-06; 13. ZKA79-11-09; 14. ZKA79-11-11;. 15. ZKA79-11-12; 16. typical seawater; 17. river water; 18. upper crust. Typical seawater, river water and upper crust data are also plotted in the diagrams for comparison (after Taylor and Mclennan, 1981, 1985; Elderfield and Greaves, 1982; Hoyle et al., 1984).

Table 2. REE data for the sandstone-type uranium deposit samples from the Ordos Basin (μg/g)

Sample No.	La	Ce	Pr	Nd	Sm	Eu	Gd	Tb	Dy	Ho	Er	Tm
GSR-4	28.5	48.1	6.34	23.9	5.58	1.00	4.70	0.77	3.84	0.73	2.09	0.32
GSR-5	59.8	100.7	12.8	44.2	8.01	1.73	6.52	1.10	6.01	1.23	3.78	0.60
ZK183-79-02	38.8	63.6	7.69	26.2	4.30	2.06	3.64	0.52	2.42	0.47	1.35	0.21
ZK183-79-06	21.4	33.0	4.26	15.4	2.90	2.00	2.47	0.40	1.99	0.39	1.13	0.16
ZK183-79-09	36.5	53.1	8.31	31.4	6.51	2.33	5.50	0.99	5.67	1.16	3.44	0.56
ZK183-79-12	19.8	21.7	4.03	14.2	2.47	1.67	2.16	0.34	1.90	0.40	1.19	0.20
ZK341-60-04	19.9	25.8	3.85	13.3	2.38	1.95	2.00	0.29	1.48	0.28	0.85	0.13
ZK341-60-05	104	153	21.1	73.0	11.85	2.72	10.26	1.70	9.08	1.87	5.60	0.89
ZK64-127-S-07	40.8	62.8	8.93	32.1	5.27	1.49	3.58	0.45	2.04	0.40	1.32	0.22
ZKA139-35-03	25.6	32.9	5.52	20.5	4.17	1.86	4.01	0.73	4.53	1.04	3.30	0.52
ZKA139-35-05	68.7	99.2	13.98	46.1	7.28	1.71	6.49	1.07	5.95	1.32	4.08	0.66
ZKA139-35-13	17.4	23.4	3.80	13.2	2.37	1.51	2.33	0.40	2.12	0.44	1.41	0.24
ZKA183-87-02	62.0	94.2	13.01	44.2	6.63	1.88	6.20	1.00	5.24	1.12	3.34	0.52
ZKA183-87-08	41.1	44.4	7.31	23.2	4.09	1.61	3.74	0.62	3.28	0.68	1.99	0.32
ZKA183-87-09	29.3	44.3	6.49	22.6	3.97	1.52	3.30	0.54	2.86	0.66	1.98	0.34
ZKA183-87-10	176.4	249.9	33.39	107.6	16.17	2.02	14.81	2.25	11.03	2.39	7.30	1.22
ZKA39-14-02	61.3	106.5	11.80	41.0	7.08	1.62	5.95	1.00	5.07	0.99	2.93	0.47
ZKA39-14-04	41.3	53.3	7.76	27.3	4.71	1.89	3.84	0.62	3.30	0.72	2.18	0.36
ZKA39-14-06	11.2	11.6	2.59	9.31	1.70	0.89	1.33	0.23	1.35	0.29	0.90	0.17
ZKA79-11-05	41.9	75.6	9.31	33.4	6.16	1.52	5.06	0.89	4.79	1.01	2.94	0.47
ZKA79-11-09	27.7	31.8	5.58	19.4	3.55	1.45	2.87	0.53	2.93	0.62	1.84	0.31
ZKA79-11-11	8.77	8.96	1.67	5.88	1.14	1.01	0.97	0.20	0.95	0.19	0.69	0.12
ZKA79-11-12	28.6	41.8	5.49	19.1	3.47	1.52	2.72	0.46	2.36	0.50	1.57	0.26

Sample No.	Yb	Lu	Y	ΣREE	ΣLa-Nd	ΣSm-Ho	ΣEr-Y	LREE/HREE	ΣCe/ΣY	δEu
GSR-4	1.81	0.23	18.4	146.4	106.9	16.62	22.89	12.07	4.19	0.83
GSR-5	3.54	0.45	38.9	289.3	217.5	24.60	47.27	13.98	4.20	0.91
ZK183-79-02	1.14	0.15	11.4	163.9	136.2	13.40	14.27	23.43	8.27	1.18
ZK183-79-06	0.94	0.13	10.2	96.7	74.0	10.14	12.55	15.83	5.31	1.37
ZK183-79-09	3.24	0.41	28.0	187.0	129.3	22.16	35.60	9.29	3.31	1.06
ZK183-79-12	1.19	0.15	8.84	80.3	59.8	8.94	11.57	12.30	4.65	1.37
ZK341-60-04	0.83	0.11	6.23	79.5	62.9	8.38	8.15	17.46	6.79	1.49
ZK341-60-05	5.29	0.67	44.7	445.7	351.2	37.48	57.10	14.98	5.39	0.93
ZK64-127-S-07	1.39	0.19	9.64	170.5	144.5	13.23	12.76	25.79	9.90	1.02
ZKA139-35-03	3.16	0.40	37.0	145.3	84.5	16.34	44.41	6.91	1.86	1.12
ZKA139-35-05	3.89	0.49	26.8	287.7	227.9	23.82	35.95	13.94	5.50	0.92
ZKA139-35-13	1.38	0.17	9.63	79.8	57.8	9.17	12.83	10.38	4.05	1.31
ZKA183-87-02	3.11	0.38	32.4	275.2	213.3	22.07	39.79	15.50	4.84	0.97
ZKA183-87-08	1.77	0.23	18.2	152.5	116.0	14.02	22.51	14.11	4.63	1.09
ZKA183-87-09	1.97	0.26	16.2	136.3	102.7	12.85	20.75	12.95	4.49	1.10
ZKA183-87-10	7.05	0.96	69.3	701.8	567.3	48.68	85.83	18.65	5.91	0.77
ZKA39-14-02	2.71	0.35	31.2	280.0	220.6	21.72	37.69	17.41	5.26	0.92
ZKA39-14-04	2.17	0.29	12.0	161.8	129.7	15.08	16.96	14.56	6.49	1.12
ZKA39-14-06	1.04	0.14	6.45	49.2	34.7	5.80	8.69	9.38	3.65	1.36
ZKA79-11-05	2.88	0.39	33.6	219.9	160.2	19.44	40.28	12.93	3.68	0.94
ZKA79-11-09	1.79	0.24	13.2	113.8	84.4	11.95	17.38	11.17	4.30	1.14
ZKA79-11-11	0.71	0.10	5.31	36.7	25.3	4.46	6.91	9.62	3.44	1.81
ZKA79-11-12	1.64	0.25	9.63	119.5	95.1	11.02	13.36	14.61	6.17	1.17

with one another. Negative Ce anomalies are common in almost all the samples, which are similar to those of typical seawater and river water. The Ce anomalies occur in response to the oxidation of Ce^{3+} to Ce^{4+} and

the precipitation of Ce^{4+} from solutions as CeO_2 (Elderfield and Greaves, 1982; Hoyle et al., 1984). Thus the origin of seawater or river water may be the cause of negative Ce anomaly, as is supported by Wang Zhonggang et al. (1989). Furthermore, it may be inferred that hydrothermal processes played a very important role in uranium enrichment. In both REE distribution pattern diagrams, with Eu as a boundary, the front part is like a slope while the rear part is flat. In this study, we classified the samples as 2 groups in terms of their negative Eu anomalies and positive Eu anomalies in order to address the problems of Eu anomalies. As seen in Fig. 3, LREE enrichment in the samples with negative Eu anomalies is slightly more remarkable than that in those with positive Eu anomalies.

4.2 Chondrite normalization of trace elements

Zhu Xiyang et al. (2003) once had made a study on the trace elements of the Dongsheng sandstone-type uranium deposit and found that there was a positive correlation between U enrichment and Mo, Ba, Zr and Se. Castor and Henry (2000) studied the trace elements of the uranium deposits in northwestern Nevada and southeastern Oregon, showing that the whole-rock U abundance was higher than 20 μg/g. Cox and Singer (1986) drew a conclusion that the U-rich samples were also enriched in Zr, As, Mo and other elements, slightly enriched in W, As, Sb, Pb and Tl from Painted Hills related to epithermal uranium deposits.

The results of analysis of trace elements are listed in Table 3.

From the trace element chondrite-normalized spider diagram (Fig. 4), it can be seen that the trace elements have the following characteristics:

Generally, along with the reduction of trace element incomepatibility from left to right, the normalized value tends to decrease gradually. Exceptional elements such as U, Ta, Nb, Sr, Hf and Zr have different degrees of positive or negative abnormity. Most of the samples show the same distribution pattern as the average upper crust, which indicates that they may have originated from an upper crust source; however, several trace elements have a

Table 3. The results of analysis of trace elements for the sandstone-type uranium deposit samples from the Ordos Basin (μg/g)

Sample No.	Rb	Th	U	Ta	Nb	La	Ce	Pb	Pr	Sr	Nd	Hf	Zr	Sm	Eu	Gd	Dy	Y	Er	Yb	Lu
GSR-4	1.90	2.15	2.19	1.24	1.23	1.96	1.77	1.77	1.67	0.68	1.60	0.96	1.12	1.46	1.06	1.19	1.00	0.96	0.92	0.86	0.79
GSR-5	2.80	2.58	2.14	1.75	1.74	2.28	2.09	1.89	1.97	1.05	1.87	1.20	1.34	1.62	1.30	1.33	1.20	1.29	1.18	1.15	1.07
ZK183-79-02	2.41	2.21	2.20	1.49	1.40	2.09	1.89	2.06	1.75	1.50	1.64	0.84	0.94	1.35	1.38	1.08	0.80	0.76	0.73	0.66	0.58
ZK183-79-06	2.37	1.80	1.85	1.31	1.19	1.83	1.61	1.96	1.49	1.54	1.41	1.29	1.22	1.18	1.36	0.91	0.72	0.71	0.66	0.58	0.53
ZK183-79-09	2.33	2.01	2.64	1.71	1.59	2.06	1.81	2.23	1.78	1.47	1.72	1.03	1.18	1.53	1.43	1.25	1.17	1.15	1.14	1.12	1.03
ZK183-79-12	2.29	1.74	3.42	1.40	1.28	1.80	1.43	1.97	1.47	1.41	1.38	0.88	1.02	1.11	1.28	0.85	0.70	0.65	0.68	0.68	0.60
ZK341-60-04	2.34	1.67	1.75	1.41	1.36	1.80	1.50	2.06	1.45	1.29	1.35	1.25	1.24	1.09	1.35	0.81	0.59	0.49	0.53	0.52	0.45
ZK341-60-05	2.48	2.66	2.52	1.84	1.83	2.52	2.28	2.42	2.19	1.23	2.09	1.36	1.49	1.79	1.49	1.53	1.38	1.35	1.35	1.33	1.25
ZK64-127-S-07	2.60	2.18	2.38	1.51	1.51	2.11	1.89	2.17	1.81	1.13	1.73	1.07	1.17	1.44	1.23	1.07	0.73	0.68	0.72	0.75	0.69
ZKA139-35-03	2.46	2.04	1.75	1.50	1.51	1.91	1.61	2.10	1.61	1.58	1.54	0.87	1.01	1.34	1.33	1.12	1.08	1.27	1.12	1.10	1.02
ZKA139-35-05	2.21	2.52	3.84	2.05	2.09	2.34	2.09	2.26	2.01	1.38	1.89	1.35	1.51	1.58	1.29	1.33	1.19	1.13	1.21	1.20	1.11
ZKA139-35-13	2.32	1.85	2.82	1.64	1.60	1.74	1.46	2.08	1.44	1.45	1.34	1.13	1.14	1.09	1.24	0.88	0.75	0.68	0.75	0.75	0.66
ZKA183-87-02	2.52	2.36	2.25	1.82	1.79	2.29	2.06	2.30	1.98	1.47	1.87	1.21	1.37	1.54	1.33	1.31	1.14	1.21	1.13	1.10	1.00
ZKA183-87-08	2.43	1.98	3.80	1.40	1.54	2.12	1.74	1.94	1.73	1.40	1.59	0.94	1.17	1.33	1.27	1.09	0.93	0.96	0.90	0.85	0.78
ZKA183-87-09	2.49	2.14	4.06	1.74	1.78	1.97	1.74	2.27	1.68	1.47	1.58	1.21	1.43	1.32	1.24	1.03	0.87	0.91	0.90	0.90	0.83
ZKA183-87-10	2.28	3.13	3.65	2.22	2.44	2.75	2.49	2.32	2.39	1.38	2.26	2.08	2.36	1.93	1.37	1.68	1.46	1.54	1.47	1.45	1.40
ZKA39-14-02	2.51	2.54	2.41	1.94	1.77	2.29	2.12	2.30	1.94	1.45	1.84	1.60	1.58	1.57	1.27	1.29	1.12	1.19	1.07	1.04	0.96
ZKA39-14-04	2.26	1.75	2.39	1.49	1.20	2.12	1.82	2.14	1.75	1.41	1.66	0.91	0.94	1.39	1.34	1.10	0.94	0.78	0.94	0.94	0.88
ZKA39-14-06	2.08	1.85	3.39	1.50	1.52	1.55	1.16	1.94	1.28	1.32	1.19	0.93	1.02	0.95	1.01	0.64	0.55	0.51	0.56	0.62	0.56
ZKA79-11-05	2.50	2.55	2.19	1.78	1.78	2.12	1.97	2.38	1.83	1.54	1.75	1.20	1.30	1.51	1.24	1.22	1.10	1.23	1.07	1.06	1.01
ZKA79-11-09	2.28	1.94	3.92	1.42	1.46	1.94	1.59	2.18	1.61	1.44	1.51	1.18	1.12	1.27	1.22	0.97	0.89	0.82	0.87	0.86	0.80
ZKA79-11-11	2.27	1.72	3.73	1.37	1.41	1.44	1.04	1.87	1.09	1.36	0.99	1.03	1.04	0.77	1.07	0.50	0.40	0.42	0.44	0.45	0.40
ZKA79-11-12	2.34	1.94	3.74	1.59	1.57	1.96	1.71	2.09	1.60	1.41	1.51	0.97	1.11	1.26	1.24	0.95	0.79	0.68	0.80	0.82	0.83

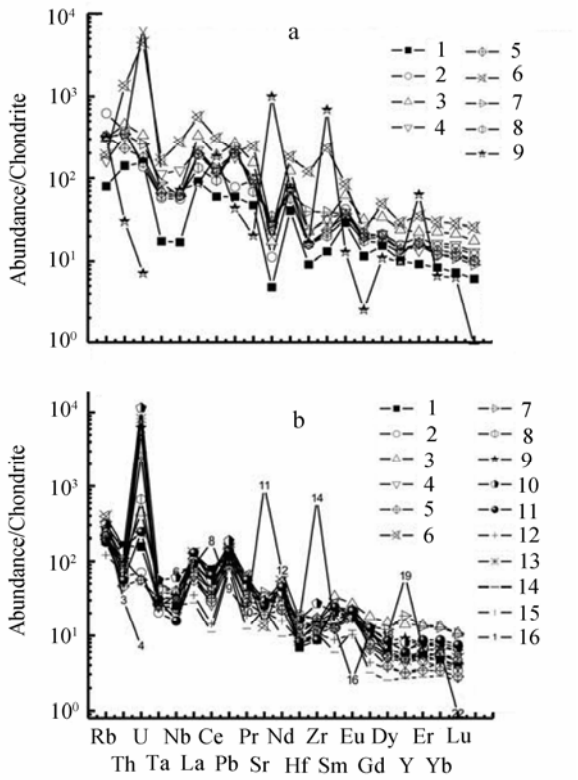

Fig. 4. Trace element chondrite-normalized spider diagram. a. Samples with negative Eu anomalies: 1. GSR-4; 2. GSR-5; 3. ZK341-60-05; 4. ZKA139-35-05; 5. ZKA183-87-02; 6. ZKA183-87-10; 7. ZKA39-14-02; 8. ZKA79-11-05; 9. upper crust. b. Samples with positive Eu anomalies: 1. ZK183-79-02; 2. ZK183-79-06; 3. ZK183-79-09; 4. ZK183-79-12; 5. ZK341-60-04; 6. ZK64-127-S-07; 7. ZKA139-35-03; 8. ZKA139-35-13; 9. ZKA183-87-08; 10. ZKA183-87-09; 11. ZKA39-14-04; 12. ZKA39-14-06; 13. ZKA79-11-09; 14. ZKA79-11-11; 15. ZKA79-11-12; 16. upper crust. The abscissa of the trace element chondrite-normalized spider diagram marks the trace elements arranged in such an order that trace element incompatibility reduces from left to right (Wang Zhonggang et al., 1989). Average upper crust data are also shown in the diagram (Taylor and Mclennan, 1981); Rb, Th, U, Ta, Nb, La, Ce, Pb, Sr, Nd, Zr, Sm and Y are after Sun and McDonough (1989); Pr, Eu, Gd, Dy, Er, Yb and Lu are after Taylor and Mclennan (1985); Hf is after Thompson (1982).

notable diversity: the abundances of Rb, U, La, Ce, Sr, Nd, Zr, Y, Pb and Pr are higher than those of others; especially Rb, U, La, Ce, Pb and Pr which show particularly positive abnormities. The abundance of U ranges widely from 0.73 to 150 μg/g. For example, 3 samples from drill ZKA183 have the highest abundance of U between 58.1–150, whereas the abundance of Th is relatively low, varying from 2.34 to 67.75 μg/g. Uranium abundance is negatively correlated with Th abundance, as is seen in Fig. 4. In Fig. 4a and b it can be seen that the samples with positive Eu anomalies are, in more cases, much higher in U abundance than those with negative Eu anomalies. Of course, more data are needed to prove it to be a universal phenomenon. The samples with negative Eu anomalies are low in Sr abundance compared with those with positive Eu samples, and it is possibly the result of Eu incompatibility; late hydrothermal activities made this phenomenon even more remarkable.

4.3 Discussion on correlations between U, Th and other trace and major elements

In this study, 14 plots showing the correlations (Fig. 5a–n) between U, Th and other trace and major elements are made to probe into the extensive correlations concerning uranium enrichments.

Figure 5a shows variations between ΣREE and U, and Th, respectively, from which a clear linear correlation trend can be found, indicating a correlation between Th and ΣREE; however, in Figure 5b, a clear linear correlation trend is shown between ΣREE and Th. Usually, the abundances of Th in medium- and coarse-grained sandstones are lower than those of fine-grained sandstones. Figure 5c shows a variation trend for Th and U, from which it can be seen that the U abundance is obviously divided into 2 parts by 10μg/g, and the abundances of U in the medium- and coarse-grained sandstones are slightly higher than those of fine-grained sandstones. Figure 5d is a ΣREE-Th/U plot, with no obvious correlation observed. Figure 5e is a plot showing variations in Rb and U; all the data points are basically at the same level, so we can infer that U enrichment is not correlated with Rb. Figure 5f is a Sr-U plot; the situation of Sr is similar to Rb and no remarkable correlation is found. Figure 5g is a Ti-U plot; a comparatively precise correlation is shown in the figure, especially for the fine-grained sandstones. Figure 5h is a Fe-U plot; the Fe abundance of each sample is relatively high, and there is no distinct correlation between Fe and U. Figure 5i is a V-U plot, with no clear correlation observed. Probably, more data are needed to support the linear correlation. Figure 5j is a Zr-U plot; medium- and coarse-grained sandstones and fine-grained sandstones have more or less corresponding correlations, respectively, though the correlations are not so clear. Figure 5k is a Mo-U plot; U abundance is obviously correlated with Mo abundance, especially for the medium- and coarse-grained-sandstones. Figure 5l is a Pb-U plot, with no clear correlation seen. Figure 5m is a Au-U plot; the medium- and coarse-grained sandstones and fine-grained sandstones show good correlations, respectively. Figure 5n is a Pd-U plot, with no obvious correlation between Pd and U.

Based on the trace element data, such a conclusion can be drawn that there exist obvious

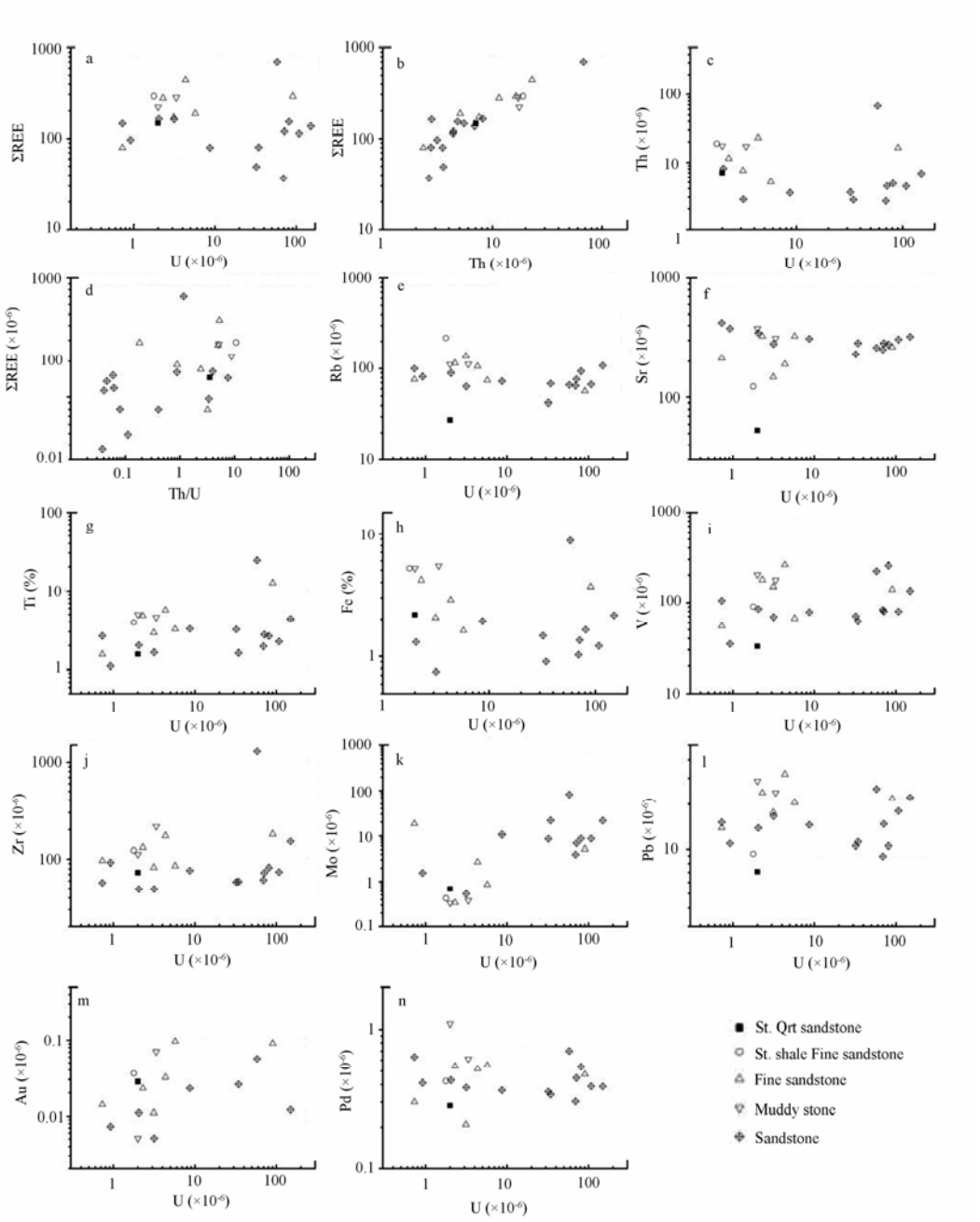

Fig. 5. Correlations between U, Th and other REE and trace elements. a. ΣREE-U correlation diagram; b. ΣREE-Th correlation diagram; c. Th-U correlation diagram; d. ΣREE-Th/U correlation diagram; e. Rb-U correlation diagram; f. Sr-U correlation diagram; g. Ti-U correlation diagram; h. Fe-U correlation diagram; i. V-U correlation diagram; j. Zr-U correlation diagram; k. Mo-U correlation diagram; l. Pb-U correlation diagram; m. Au-U correlation diagram; n. Pd-U correlation diagram.

positive correlations between U and other trace elements such as Ti, V, Zr, Mo, Au and so on. Therefore, the elements Ti, V, Zr, Mo, and Au can be considered as an indicator of uranium enrichment. In addition, Th abundance is obviously correlated with ΣREE. This has been proved by the data from other metallic ore deposits. Bao Zhiwei and Zhao Zhenhua (2003) studied the rare-earth element mobility during ore-forming hydrothermal alteration and found that the mobility and fractionation of REE and the coherent mobilities of Y, U, Th and Au lend great support to the hypothesis that syenite is one of the source rocks for gold mineralization.

5 Conclusions

Through the extensive analysis and discussion of REE and trace elements in the sandstone-type uranium

deposits in the Ordos Basin, we have drawn the following conclusions:

(1) The sandstone-type uranium deposits in the Ordos Basin are characterized by light REE enrichment and heavy REE depletion; ΣREE fluctuates awfully between 36.7 μg/g and 701.8 μg/g; Eu anomalies vary greatly from 0.77 to 1.81. The statistics data for ΣLa-Nd, ΣSm-Ho and ΣEr-Y indicate obvious LREE enrichment, slight MREE depletion and strong HREE depletion. Based on the Eu and Ce anomalies, it is obvious that late-stage hydrothermal activities had occurred and played a very important role in uranium enrichment.

(2) The abundances of Rb, U, La, Ce, Sr, Nd, Zr, Y, Pb and Pr are relatively high, and especially the elements Rb, U, La, Ce, Pb and Pr show positive anomalies. Higher U abundance vs. lower Sr abundance is a universal phenomenon, as revealed in this study. There exist obvious positive correlations between U and other trace elements such as Ti, V, Zr, Mo, and Au, whereas Th abundance is obviously correlated with ΣREE.

(3) The study has revealed an important relationship between the U and Th abundances and the granularities of rocks, i.e., the concentrations of Th in the medium and coarse-grained sandstones are lower than those of the fine-grained sandstones. However, this case is not true for U concentrations.

Acknowledgements The authors wish to extend their sincere thanks to Professor Yu Huaming and his assistants with the Physics and Chemistry Laboratory Center of the University of Science and Technology of China for their help with REE and trace element analysis.

References

Bao Zhiwei and Zhao Zhenhua (2003) Rare-earth element mobility during ore-forming hydrothermal alteration, A case study of the Dongping gold deposit, Hebei Province, China [J]. *Chinese Journal of Geochemistry.* **22**, 45–57.

Castor S.B. and Henry C.D. (2000) Geology, geochemistry and origin of volcanic rock-hosted uranium deposits in northwestern Nevada and southeastern Oregon [J]. *Ore Geology Reviews*. **16**, 1–40.

Chen Daisheng, Li Shengxiang, and Cai Yuqi (2003) A discussion on research situation and development direction of and stone-type uranium deposits in the Meso-Cenozoic basins of China [J]. *Acta Sedimentologica Sinica.* **21**, 113–117 (in Chinese with English abstract).

Cheng Fazheng (2002) Analysis on paleohydrogeologic conditions and prospects of uranium metallogenesis in the northern part of the Ordos Basin [J]. *Uranium Geology*. **18**, 287–294 (in Chinese with English abstract).

Cox D.P. and Singer D.A. (1986) Mineral deposit models [J]. *US Geological Survey Bulletin*. **1693**, 379.

Dai Jinxing, Li Jian, Luo Xia, Zhang Wenzheng, and Hu Guoyi (2005) Alkane carbon isotopic composition and gas source in giant gas fields of the Ordos Basin [J]. *Acta Petrolei Sinica.* **26**, 18–26 (in Chinese with English abstract).

Darby B.J. and Ritts B.D. (2002) Mesozoic contractional deformation in the middle of the Asian tectonic collage, the intraplate Western Ordos fold-thrust belt, China [J]. *Earth and Planetary Science Letters.* **205**, 13–24.

Di Yongqiang (2002) Preliminary discussion on prospecting potential for sandstone-type uranium deposits in Meso-Cenozoic basins, northern Ordos [J]. *Uranium Geology*. **18**, 340–347 (in Chinese with English abstract).

Elderfield H. and Greaves M.J. (1982) The rare-earth elements in seawater [J]. *Nature*. **296**, 214–219.

Fleet A.R. (1984) Aqueous and sedimentary geochemistry of the rare-earth elements. In *Rare-Earth Element Geochemistry* (ed. P. Henderson) [M]. pp. 331–373. Elsevier, London.

Granger H.C., Santos E.S., Dean B.G., and Moore F.B. (1961) Sandstone-type uranium deposits at Ambrosia Lake, New Mexico: An interim report [J]. *Economic Geology*. **56**, 1179–1209.

Hoyle J., Elderfield H., Gledhill A., and Greaves M. (1984) The behavior of the rare-earth elements during the mixing of river and seawaters [J]. *Geochim. Cosmochim. Acta.* **48**, 143–149.

Hu Wenrui (2000) *Theory and Technique of Oil-Gas Prospecting and Exploration Exploitation in the Ordos Basin* [M]. pp. 1–4. Changqing Petroleum Exploration Bureau, China National Petroleum Corporation (in Chinese).

Li Shengfu and Zhang Yun (2004) Formation mechanism of uranium minerals at sandstone-type uranium deposits [J]. *Uranium Geology*. **20**, 80–84 (in Chinese with English abstract).

Li Xianqing, Hou Dujie, Hu Guoyi, Liu Changqing, and Tang Youjun (2003a) Characteristics of organic components in formation waters and their relations to natural gas reservoirs in central Ordos Basin [J]. *Chinese Journal of Geochemistry*. **22**, 116–122.

Li Xianqing, Hou Dujie, Tang Youjun, Hu Guoyi, and Xiong Bo (2003b) Molecular geochemical evidence for the origin of natural gas from dissolved hydrocarbons in Ordovician formation waters in central Ordos Basin [J]. *Chinese Journal of Geochemistry*. **22**, 193–202.

Liu Chiyang (2005) *Advances in the Accumulation and Formation for Multi-Energy Mineral Deposits Coexisting in the Same Basin* [M]. pp. 1–16. Science Press, Beijing (in Chinese).

Liu Chiyang, Zhao Hongge, Wang Feng, and Chen Hong (2005) Mesozoic structure properties of the Ordos Basin western edge (middle part) [J]. *Acta Geologica Sinica.* **79**, 737–747 (in Chinese with English abstract).

Liu Shaofeng (1998) The coupling mechanism of basin and orogen in the western Ordos Basin and adjacent regions of China [J]. *Journal of Asian Earth Sciences.* **16**, 369–383.

Liu Ying, Liu Haichen, and Li Xianhua (1996) Simultaneous and precise determination of 40 trace elements in rock samples using ICP-MS [J]. *Geochimica*. **25**, 552–558 (in Chinese with English abstract).

McLennan S.M. (1989) Rare-earth elements in sedimentary rocks, influence of provenance and sedimentary processes. In *Geochemistry and Mineralogy of Rare-Earth Elements* (eds. B.R. Lipin and G.A. McKay) [C]. Min. Soc. Am. Rev. Mineral. **21**, 169–200.

Milodowski A.E., West J.M., Pearce J.M., Hyslop E.K., Basham I.R., and Hooker P.J. (1990) Uranium-mineralized microorganisms associated

with uraniferous hydrocarbons in southwest Scotland [J]. *Nature.* **347**, 465–467.

Min Maozhong, Xu Huifang, Chen Jia, and Mostafa Fayek (2005) Evidence of uranium biomineralization in sandstone-hosted Roll-Front uranium deposits, northwestern China [J]. *Ore Geology Reviews.* **26**, 198–206.

Peng Xinjian, Min Maozhong, Wang Jinping, Jia Heng, Wei Guanhui, and Wang Jianfeng (2003) Characteristics and geochemical significance of the ferrum phase in the Shihongtan interlayered-oxidation zone sandstone-type uranium deposit [J]. *Uranium Geology*. **77**, 120–125 (in Chinese with English abstract).

Ritts B.D., Hanson A.D., Darby B.J., Nanson L., and Berry A. (2004) Sedimentary record of Triassic intraplate extension in North China, evidence from the non-marine NW Ordos Basin, Helan Shan and Zhuozi Shan [J]. *Tectonophysics*. **386**, 177–202.

Sun S.S. and McDonough W.F. (1989) Chemical and isotopic systematics of oceanic basalts, implications for mantle composition and processes. In *Magmatism in the Ocean Basins* (eds. A.D. Saunders. and M.J. Norry) [M]. pp. 313–345. Geological Society of London, London.

Taylor S.R. and Mclennan S.M. (1981) The composition and evolution of the continental crust: Rare-earth element evidence from sedimentary rocks [J]. *Phil. Trans. R. Soc.* **A301**, 381–399.

Taylor S.R. and Mclennan S.M. (1985) *The Continental Crust, Its Composition and Evolution* [M]. pp. 9–56. Blackwell, Oxford.

Thompson R.N. (1982) British Tertiary volcanic province [J]. *Scottish Journal of Geology*. **18**, 59–107.

Wang Zhonggang, Yu Xueyuan, and Zhao Zhenhua (1989) *Rare-Earth Element Geochemistry* [M]. pp. 1–535. Science Press, Beijing (in Chinese).

Wei Yongpei and Wang Yi (2004) Comparison of enrichment patterns of various energy resources in the Ordos Basin [J]. *Oil & Gas Geology*. **25**, 385–392 (in Chinese).

Wu Rengui, Chen Anping, Yu Dagan, Zhu Minqiang, and Zhou Wanpeng (2003) Analysis on depositional system and discussion on ore formation conditions of channel sandstone-type uranium deposits—taking Dongsheng area, Ordos Meso-Cenozoic basin as an example [J]. *Uranium Geology*. **19**, 94–99 (in Chinese with English abstract).

Xia Yuliang, Lin Jingrong, Liu Hanbin, Fan Guang, and Hou Yanxian (2003) Research on geochronology of sandstone-hosted uranium ore-formations in major uranium-productive basins, northern China [J]. *Uranium Geology*. **19**, 129–136 (in Chinese with English abstract).

Xiao Xinjian, Li Ziying, and Chen Anping (2004a) Preliminary study on features of mineralogical zoning of epigenetic alteration at sandstone-type uranium deposit, Dongsheng area, Ordos Basin [J]. *Uranium Geology*. **20**, 137–140 (in Chinese with English abstract).

Xiao Xinjian, Li Ziying, Fang Xiheng, Ou Guangxi, Sun Ye, and Chen Anping (2004b) The evidence and significance of epithermal mineralization fluid in the Dongsheng sandstone-type uranium deposit [J]. *Bulletin of Mineralogy, Petrology and Geochemistry*. **23**, 301–304 (in Chinese with English abstract).

Xie Chenxia (2004) Recent significant gas discoveries in China, influence on national energy structure and future gas exploration [J]. *Search and Discovery Article,* #10067 (see: http://www.searchanddiscoverynet/documents/2004/xie/index.htm).

Yang Dianzhong, Xia Bin, and Wu Ganguo (2004) Development characteristics of interlayer oxidation zone type of sandstone uranium deposits in southwestern Turfan-Hami Basin [J]. *Science in China* (Ser. D). **47**, 419–426.

Yang Xiaoyong, Ling Mingxing, Sun Wei, Miao Jianyu, and Liu Chiyang (2006) Study on the fluid inclusions from the sandstone-type uranium deposits in the Ordos Basin: Their significance [J]. *Acta Petrolei Sinica*. (in press, in Chinese with English abstract).

Ye J.R. and Lu M.D. (1997) Geochemistry modeling of cratonic basin: A case study of the Ordos Basin, NW China [J]. *Journal of Petroleum Geology.* **20**, 347–362.

Zhang Jin, Ma Zongjin, and Ren Wenjun (2004) Tectonic characteristics of the western Ordos thrust-fold belt and the causes for its north-south segmentation [J]. *Acta Geologica Sinica*. **78**, 600–611 (in Chinese with English abstract).

Zhang Lifei, Sun Min, Wang Shiguang, and Yu Xueyuan (1998) The composition of shales from the Ordos Basin, China, Effects of source weathering and diagenesis [J]. *Sedimentary Geology*. **116**, 129–141.

Zhao Zhongyuan and Liu Chiyang (1990) *The Forming and Evolution of North China Craton Depositional Basin and Hydrocarbon Accumulation* [M]. Northwest Univ. Press, Xi'an (in Chinese).

Zhu Xiyang, Wang Yunliang, Wang Zhichang, Zhang Chengjiang, and Liu Jianhua (2003) Trace element geochemistry of sandstone-type uranium deposits in the Dongsheng area [J]. *Geology & Geochemistry.* **31**, 39–45 (in Chinese with English abstract).